New sol-gel formulations to increase the barrier effect of a protective coating against the corrosion of steels

Elise Certhoux, Florence Ansart, Viviane Turq, Jean Pierre Bonino, Jean Michel Sobrino, Julien Garcia, Jean Reby

New sol–gel formulations to increase the barrier effect of a protective coating against the corrosion of steels

E. Certhoux[a], F. Ansart[a] *, V. Turq[a], J.P. Bonino[a], J.M. Sobrino[b], J. Garcia[b], J. Reby[c]

[a] Institut Carnot CIRIMAT, Université de Toulouse, UMR 5085, 118 Route de Narbonne, 31062 Toulouse Cedex 9, France
[b] Institut Carnot CETIM, Pôle Matériaux Métalliques et Surfaces, 52 av. Félix Louat - BP 80067, 60304 Senlis Cedex, France
[c] Institut Carnot CETIM, Pôle Matériaux Métalliques et Surfaces, 74 route de La Jonelière - BP 82617, 44326 Nantes Cedex 3, France

Keywords:

Steel
Protection
Sol–gel route
Adhesion
Plasticizer

A B S T R A C T

Films were deposited onto AISI 430 stainless steel substrates by dip–coating technique. The aim is to reach the AISI 304L stainless steel anti-corrosion properties by a coated AISI 430 stainless steel system. Sol formulation is done from the starting precursors tetraethylorthosilicate (TEOS) and 3(trimethoxysilyl)propyl methacrylate (MAP). After the hydrolysis of these precursors, sol–gel reactions occur before the addition (or not) of a controlled quantity of cerium nitrate. The addition of the PEG (polyethylene glycol), used as plasticizer has been studied in this paper and both physical and chemical properties of the synthesized hybrid films were studied by varying PEG ratios. Based on SEM observations and mass gain measurements, the thickness of the films has been adjustable. Another parameter plays a key role: the drying step of the whole system. It has been investigated and optimized in this paper to lead to coatings with a high barrier effect. The efficiency of the anti-corrosion protection of hybrid-coated stainless steel was investigated by potentiodynamic polarization curves and electrochemical impedance spectroscopy (EIS) after immersion of the material in a 3.5% NaCl solution.

Double-layered systems were successfully developed and a good compromise between PEG content and drying conditions has been found. Potentiodynamic polarization curves showed that the hybrid coating prepared using a TEOS/MAP/PEG yielded the best anti-corrosion performances. It acts as an efficient barrier similar to AISI 304 stainless steel used as reference, increasing the total impedance and significantly reducing the current densities.

1. Introduction

The coatings prepared via sol–gel route show interesting properties in the field of the mechanics and more generally towards the anti-corrosive protection of metal substrates. The sol–gel process is an innovating technology due to its properties of surface protection correlated to the feasibility of efficient protection via a new eco-friendly route [1–5] consisting of the hydrolysis and condensation of metal alkoxides to obtain metaloxane chains [6–9]. These chains generate sols that are then used to coat numerous metal substrates to protect them against corrosion [1–6,10–14].

The stainless steels are part of the metals most used for industrial applications against corrosion. However, the cost of stainless steels, more particularly austenitic ones (at high nickel content) undergoes strong cyclic variations of cost which is a critical problem for the manufacturers. Considering both economic and environmental aiming, it is necessary to develop coatings able to improve the corrosion resistance of low cost stainless steels (for example, ferritic ones such as AISI 430), mainly by barrier effect, to enable them to reach performances similar to the reference austenitic families (AISI 316L or AISI 304L).

The industrialization of the sol–gel process requires to work on real substrates. Also, in order to be able to protect various types of substrates by this process, with various roughnesses, it is advisable to vary the thickness of the coatings in order to keep the best possible barrier effect on all surfaces. Two routes are investigated to increase the coatings thickness. First, it is possible to increase the number of layers but within a limit to avoid delamination problems. Secondly, the viscosity of the sol can be increased, via a temperature modification but in this case, kinetics of the hydrolysis and condensation reactions varies and can induce modifications of the intrinsic properties of gel first then coating, and finally by introducing a plasticizing agent. This last route was chosen in this study because it can be easily adjustable.

So, in this study, we worked on the influence of the addition of a plasticizer, polyethylene glycol 35000 (PEG 35000) in the formulation of hybrid TEOS–MAP based sols for protection against the corrosion of stainless steel AISI 430. Electrochemical and

* Corresponding author. Tel.: +33 561 55 61 08; fax: +33 561 55 61 23.
E-mail address: ansart@chimie.ups-tlse.fr (F. Ansart).

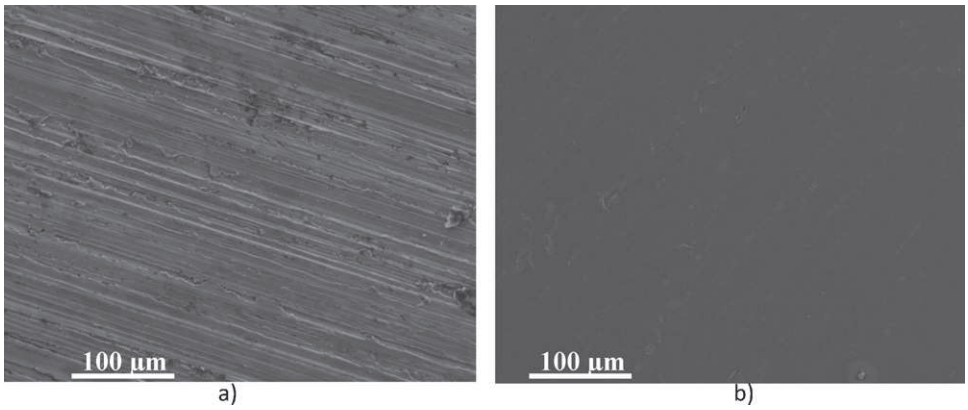

Fig. 1. Micrographs of stainless steel substrates (a) substrate R1 and (b) substrate R2.

mechanical characterizations were carried out in order to quantify the barrier effect and adherence of coatings.

2. Materials and methods

2.1. Materials

The substrate consists of stainless steel ferritic AISI 430 samples (composition in Table 1) whose dimensions are 20 mm × 80 mm × 2 mm.

Two types of substrates were studied. Their composition is similar but they have two different arithmetical mean roughnesses called R_a, measured by white light optical interferometry.

From an industrial point of view, R1 is representative of polished surfaces, R2 is representative of rough surfaces of brilliant aspect. In Fig. 1, before surface treatment and deposit, the different topographies at the same scale clearly appear.

The following experiments and characterizations were all performed on R1 substrates which is the more critical one due to the surface morphology except for the mechanical characterizations, where only deposits on R2 substrates have been characterized in order to avoid artefacts due to the roughness effect.

Before deposition, a surface preparation is necessary to obtain, at the same time, a good absorptivity of the sol and a good homogeneity of the deposits. Thus, the substrates are degreased in an alkaline bath (NaOH) at 60 °C during 20 min then pickled during 1–2 min in a solution of 50 vol% HCl.

2.2. Processing of coatings on stainless steel substrates AISI 430

The sol is prepared starting from the mixture of two silicated precursors: the tetraethylorthosilicate (TEOS) and 3-(trimethoxysilyl)propyl methacrylate (MAP). After the hydrolysis of these precursors, sol–gel reaction (hydrolysis and condensation) occurs before the cerium nitrate addition (or not) to ensure the role of corrosion inhibitor in the sol–gel matrix [24]. In fact, in this study aiming to evaluate the efficiency of plasticizers, the quantity of cerium nitrate has not been a key parameter and several

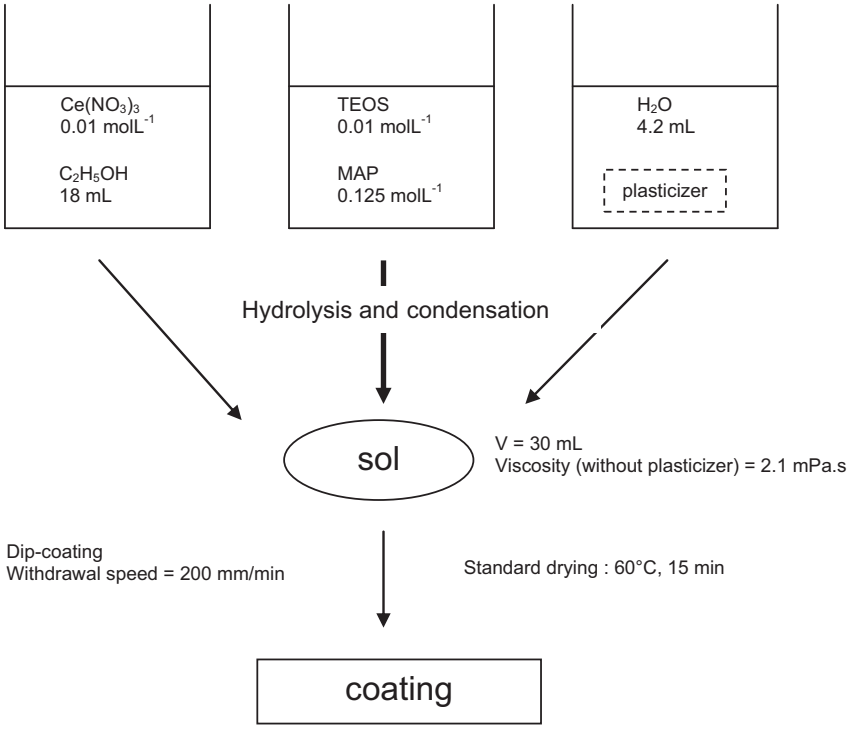

Fig. 2. Experimental parameters of synthesis of the sols and processing to deposit coatings.

Table 1
Composition of ferritic stainless steel AISI 430.

Element	Fe	Cr	Ni	Mn	Si	Mo	P	S	C
Massic percentage	82.83	16.31	0.14	0.29	0.35	0.02	0.022	0.005	0.038

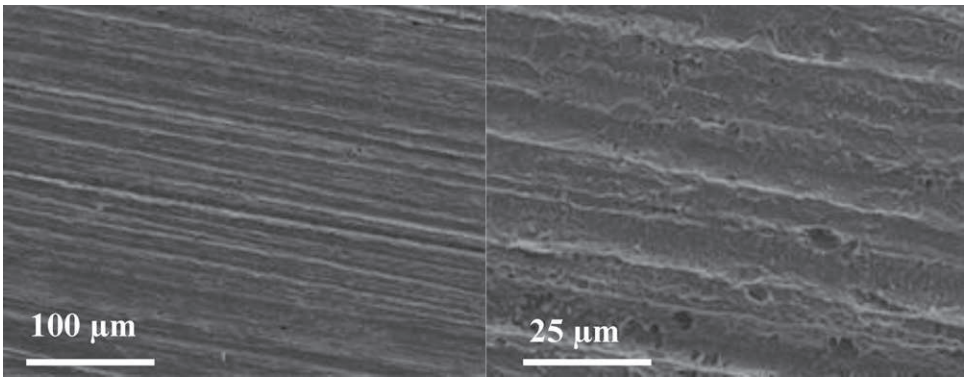

Fig. 3. Scanning electron micrographs of a TEOS–MAP coating on R1 substrate.

experiments were also performed without the incorporation of cerium. The solvents used are water and ethanol. The plasticizing agent is then added to the volume of water used for the synthesis. In this study, we have investigated several plasticizers such as sorbitol, glycerol and polyethylene glycol (PEG) 400, 1500 and 35000. After an ageing of 24 h, the coatings are deposited by dip/coating with a withdrawal speed corresponding to 200 mm min^{-1}. Thereafter, the samples are dried during 15 min at 60 °C in a drying oven. The whole protocol of the sol preparation and coatings is detailed on the flow chart (Fig. 2).

2.3. Characterization techniques

The sol viscosity is measured with a rheometer with rotary cylinder MCR 301 for shearing rates ranging between 0 and 1000 s^{-1}. The measurements of contact angles were performed with a goniometer DGC Fast 60 using deionized water. The microstructure of the coatings is analyzed using a Scanning Electron Microscope JEOL 2100F operating at 10 kV with a distance of 48 mm.

The anti-corrosion barrier properties of the coatings were evaluated by electrochemical measurements by using a corrosive 3.5% NaCl solution. The electrochemical cell of 200 mL, connected to a potentiostat PGP 201, is composed of a saturated calomel electrode, a platinum electrode and a working electrode characteristic of the studied sample. The working surface is of 1 cm^2. Before any measurement, the sample is immersed into the corrosive solution during 1 h for stabilization. The test consists in carrying out an electrochemical cycle on a potential range between a value of −1.5 and 1.5 V. Indeed, a sweeping is carried out towards the anodic potentials at the speed of 1 mV/s making it possible to determine the potential of punctures to the current density characteristic of 50 µA/cm^2. Sweeping in potential is then reversed when the current density reaches 2 mA/cm^2.

Contact angles were determined by a calibrated drop technique, using a DGD fast 60 goniometer (GBX Scientific Instruments) coupled with a software (Windrop++) to capture and analyze images. The contact angle results are the average value of at least 5 measurements at different positions on the substrate surface.

The adhesion of the coating, produced by the sol–gel route, has been evaluated using a Nano Scratch Tester by CSM Instruments at progressive load. The critical normal loads for strain or failure of the coating can be measured with this apparatus. Using the optical module of the apparatus (maximum magnification ×100), the critical normal load for cracking (CL1) or the critical normal load for spalling (CL2) can be located on the scratch track and measured [22,23]. On each sample, 3 scratches have been performed. During each scratch, the normal load increases from 0.3 to 20 mN, the loading rate is 13 mN min^{-1}, the displacement speed is 1 mm min^{-1} and the total length of the scratch is 1.5 mm. The radius of the Rockwell C diamond indenter is 2 µm. All the scratch tests have been conducted on the coating deposited on polished R2 substrate in order to minimize the effect of roughness on the results.

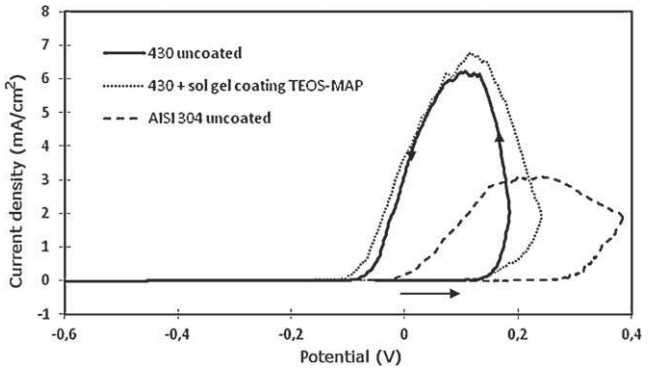

Fig. 4. Polarization curves in NaCl 3.5% for AISI 304 and AISI 430 stainless steels with and without TEOS–MAP sol–gel deposit.

3. Results and discussion

3.1. Characterization of conventional coatings without additives

Coatings containing hybrid TEOS–MAP sol were carried out on the R1 substrate because it is the more critical case due to its topography. The viscosity of the sol of 2.1 mPa s allows to obtain a mass gain of deposits of 90 mg/cm^2 but that is not sufficient to recover the entire surface topography of the substrate. Fig. 3 indeed proves that such coatings do not present the required covering effect. At a higher magnitude (right photograph – Fig. 3), areas without matter can be observed. Taking into account the arithmetical mean roughnesses, it can be deduced that the covering is not homogeneous on the surface.

This discontinuous covering is confirmed by the electrochemical tests (Fig. 4) because the barrier properties are not

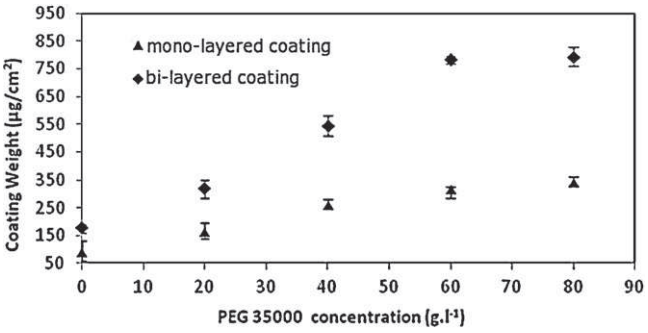

Fig. 5. Weight increase for mono and bi-layer coatings for various concentrations in PEG 35000 (standard drying: 60 °C, 15 min).

improved. Indeed, the potential read for a value of current density $J = 0.05\ mA/cm^2$ is of 0.133 V for substrate AISI 430, of 0.127 V for covered AISI 430 substrate of the sol–gel TEOS–MAP film and of 0.276 V for the stainless steel substrate austenitic AISI 304.

The barrier effect is not improved with this system because the film thickness is not sufficient. So, the objective was to increase the coatings thickness by increasing the sol viscosity via a plasticizer. Many plasticizers were tested with various concentrations [15]: sorbitol, glycerol and polyethylene glycol (PEG) 400, 1500 and 35000. The PEG 35000 was chosen thanks to its great molar mass which made it possible to significantly increase the viscosity by limiting the desorption during the drying of the deposits [16–18].

Table 2
Sol viscosity for various concentrations in PEG 35000.

Concentration in PEG 35000 ($g\,L^{-1}$)	0	20	40	60	80
Viscosity (mPa s)	2.1	4.5	8.1	11.0	12.9

3.2. Effect of the PEG 35000 concentration on the deposits morphology

The concentrations in PEG 35000 tested are: 0, 20, 40, 60, 80 $g\,L^{-1}$ and the results show that when the concentration grows, the sol viscosity increases (Table 2). Indeed with a concentration in PEG 35000 of 80 $g\,L^{-1}$ it is possible to increase by a factor of 6, the initial viscosity of a TEOS–MAP sol without plasticizer. Nevertheless, this value is a threshold value which it is not suitable to exceed to avoid problems during the processing step.

Single- and double-layered coatings were carried out with the previous sols in order to evaluate the increase of the deposits thickness.

To elaborate double-layered systems, after the first dip, the coating is simply dried (15 min, 60 °C) in order to remove the more

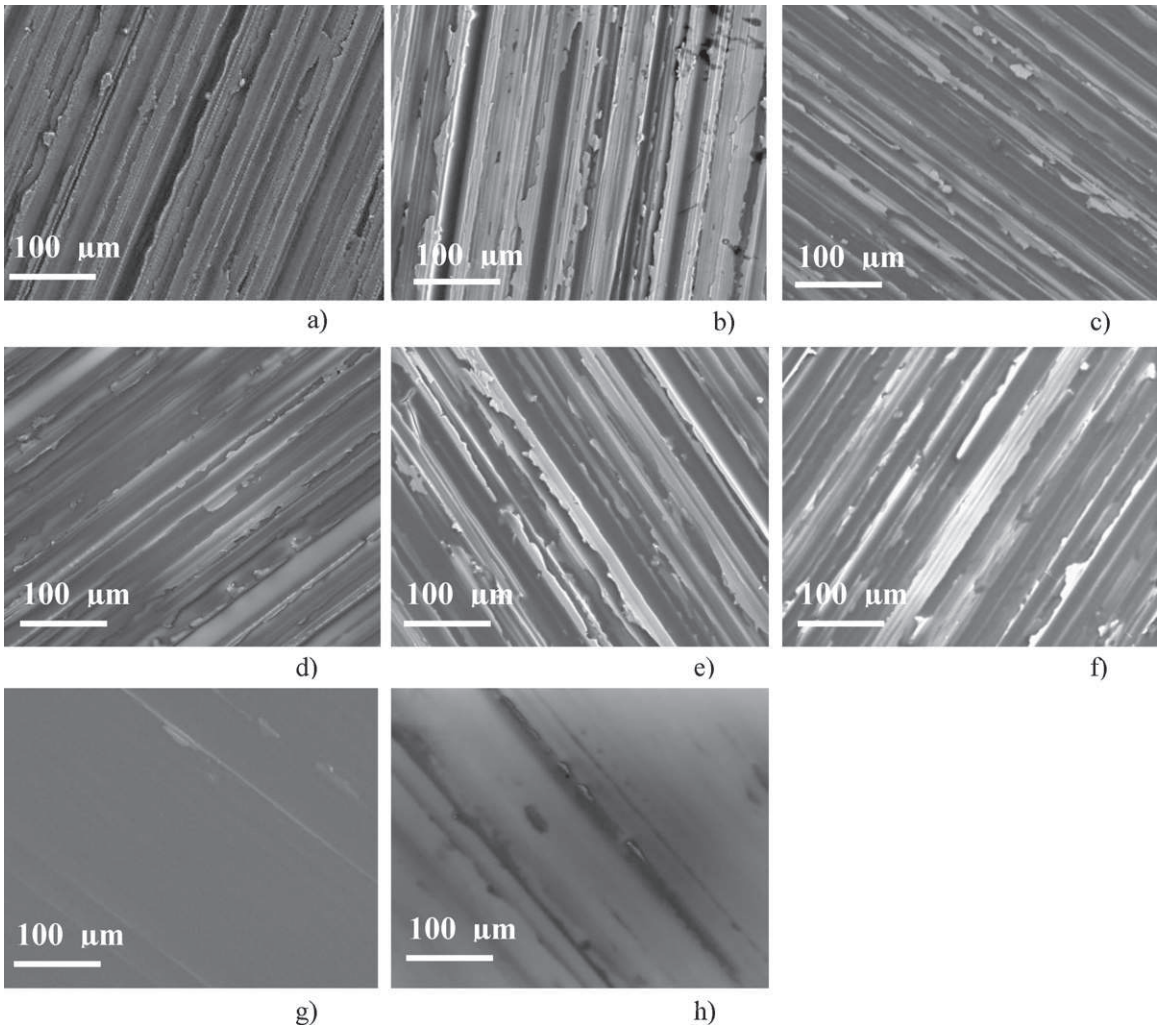

Fig. 6. Scanning electron micrographs of TEOS–MAP–PEG 35000 coatings (a) 20 $g\,L^{-1}$ 1 layer, (b) 40 $g\,L^{-1}$ 1 layer, (c) 60 $g\,L^{-1}$ 1 layer, (d) 80 $g\,L^{-1}$ 1 layer, (e) 20 $g\,L^{-1}$ 2 layers, (f) 40 $g\,L^{-1}$ 2 layers, (g) 60 $g\,L^{-1}$ 2 layers and (h) 80 $g\,L^{-1}$ 2 layers.

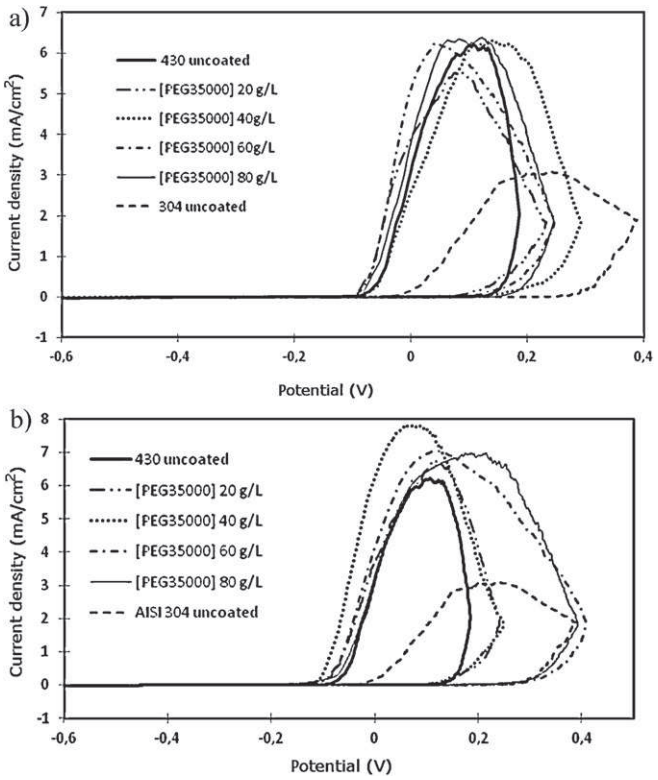

Fig. 7. Polarization curves for coatings TEOS–MAP (a) 1 layer and (b) 2 layers, for various PEG 35000 concentrations.

volatile compounds before the second dip. Weight gain measurements of the AISI 430 stainless steel samples before and after deposit are presented in Fig. 5. A clear increase in the mass gain can be underlined when the PEG 35000 concentration in the sol increases until 60 g L^{-1}. Indeed for mono-layered systems, the respective mass gain for 60 g L^{-1} and 80 g L^{-1} are 317 μg cm^{-2} and 342 μg cm^{-2} and for double-layered systems these mass gains are 785 μg cm^{-2} and 794 μg cm^{-2}.

For each experiment, a series of three analyses have always been performed.

Furthermore, Fig. 6a–d shows microstructures of the single-layered coatings with concentrations in PEG 35000 from 20 to 80 g L^{-1}. In these conditions, no coating can efficiently recover all the surface topography of the R1 substrates. Relative to double-layered coatings (Fig. 6e–h), concentrations of 60 g L^{-1} and 80 g L^{-1} lead to covering and homogeneous coatings. Polarization curves carried out on these coatings confirm these observations. Indeed, for single-layered coatings (Fig. 7a), the barrier effect is not

Table 3
Polarization tests results for various PEG 35000 concentrations.

Samples	$E_{pitting}$ (V)
Stainless steel 430 without deposit	0.133
Stainless steel 304 without deposit	0.276
Deposit TEOS–MAP + PEG 35000 (20 g L^{-1})	
1 layer	0.098
2 layers	0.130
Deposit TEOS–MAP + PEG 35000 (40 g L^{-1})	
1 layer	0.137
2 layers	0.115
Deposit TEOS–MAP + PEG 35000 (60 g L^{-1})	
1 layer	0.107
2 layers	0.281
Deposit TEOS–MAP + PEG 35000 (80 g L^{-1})	
1 layer	0.158
2 layers	0.265

Table 4
Investigated drying conditions.

Duration	15 min	30 min	60 min	120 min
Temperature	60 °C 90 °C	60 °C 90 °C	60 °C 90 °C	60 °C 90 °C

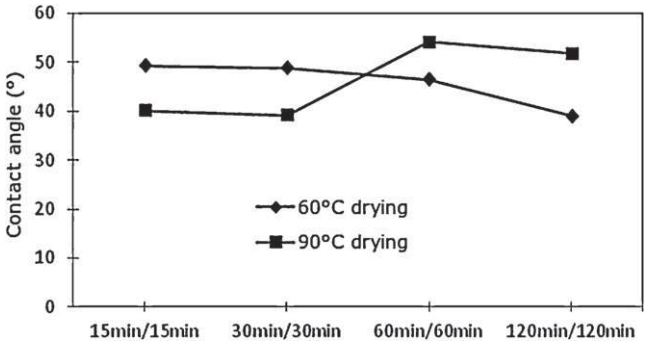

Fig. 8. Contact angle measurements for different drying conditions.

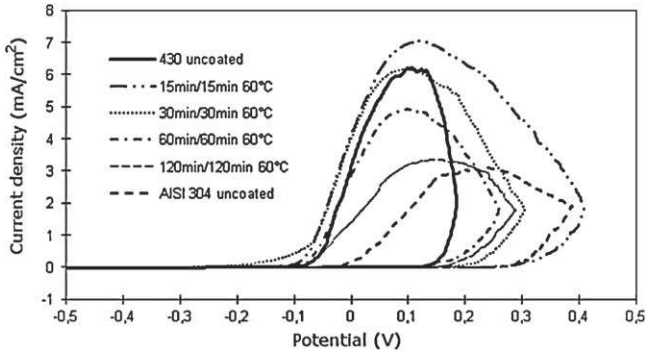

Fig. 9. Polarization curves for AISI 430 and AISI 304 substrates and for the dried coatings at 60 °C.

improved since the pitting potentials (see values in Table 3) are of the same order of magnitude as those of AISI 430 stainless steel (respectively 0.098 V; 0.137 V; 0.107 V; and 0.158 V as a function of the plasticizer concentration in comparison with 0.133 V before deposit). Nevertheless, the polarization curves of the double-layered coatings (Fig. 7b) are moved towards more anodic potentials for deposits with PEG 35000 at a concentration of 60 g L^{-1} and 80 g L^{-1}. The pitting potentials are thus higher than values of 0.281 and 0.265 V for concentrations of 60 g L^{-1} and 80 g L^{-1}, respectively. So, the objective to reach same barrier properties that AISI 304 steel has been achieved.

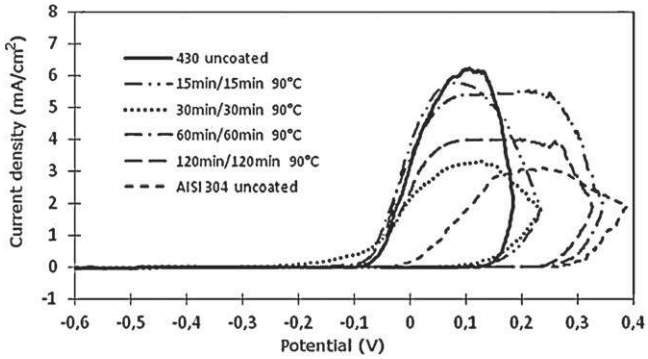

Fig. 10. Polarization curves for AISI 430 and AISI 304 substrates and of the dried coatings.

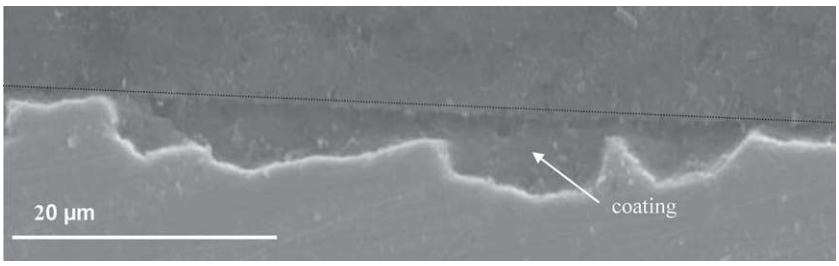

Fig. 11. Cross section of a double-layered coating (TEOS–MAP–PEG 60 g L^{-1}) 60 min drying at 90 °C.

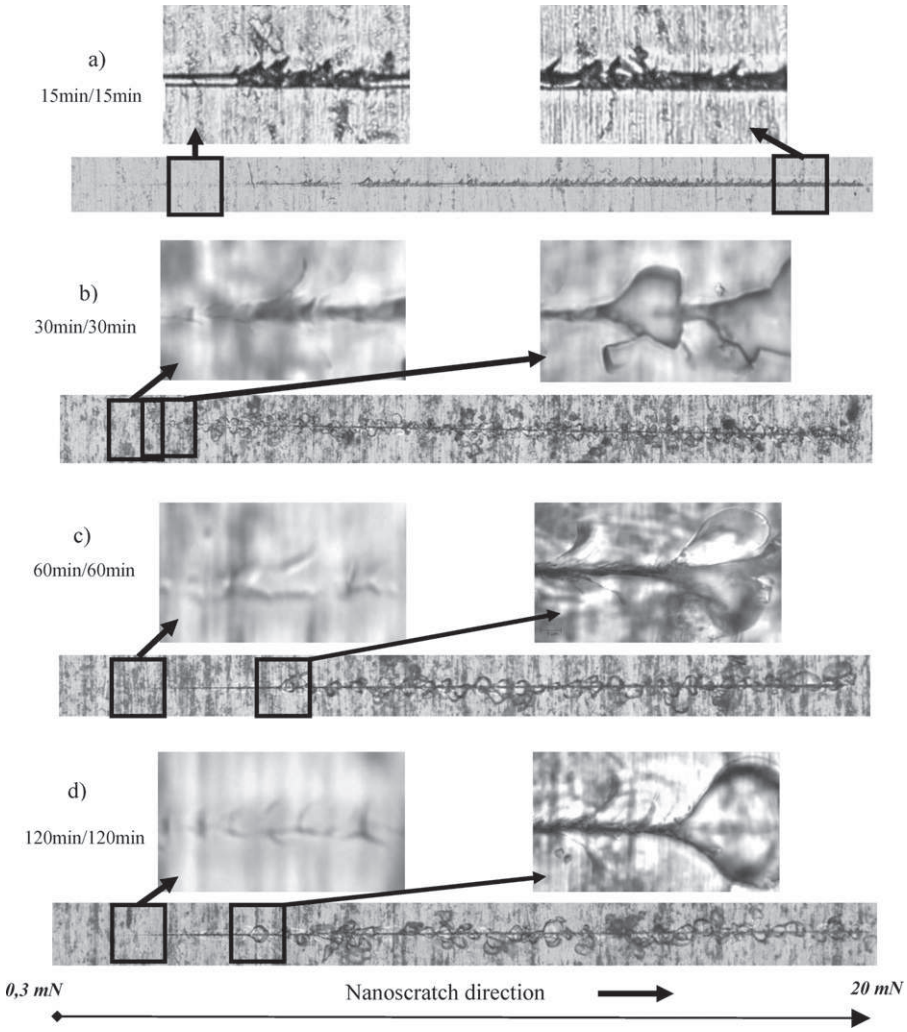

Fig. 12. Optical micrographs of nanoscratches of bi-layered coatings dried at 60 °C, (a) 15 min/15 min, (b) 30 min/30 min, (c) 60 min/60 min and (d) 120 min/120 min.

Table 5
Pitting potentials for various dryings.

Duration	15 min	30 min	60 min	120 min	
Temperature	60 °C	0.281 V	0.185 V	0.139 V	0.141 V
	90 °C	0.110 V	0.070 V	0.246 V	0.250 V

Table 6
Critical normal loads for cracking (CL1) and spalling (CL2) for the bi-layered systems.

	60 °C				90 °C			
	15 min/15 min	30 min/30 min	60 min/60 min	120 min/120 min	15 min/15 min	30 min/30 min	60 min/60 min	120 min/120 min
CL1	2.9 mN	2.0 mN	2.1 mN	2.2 mN	2.6 mN	2.2 mN	4.8 mN	5.1 mN
CL2	–	2.3 mN	5.7 mN	5.0 mN	6.4 mN	6.8 mN	14.5 mN	15.0 mN

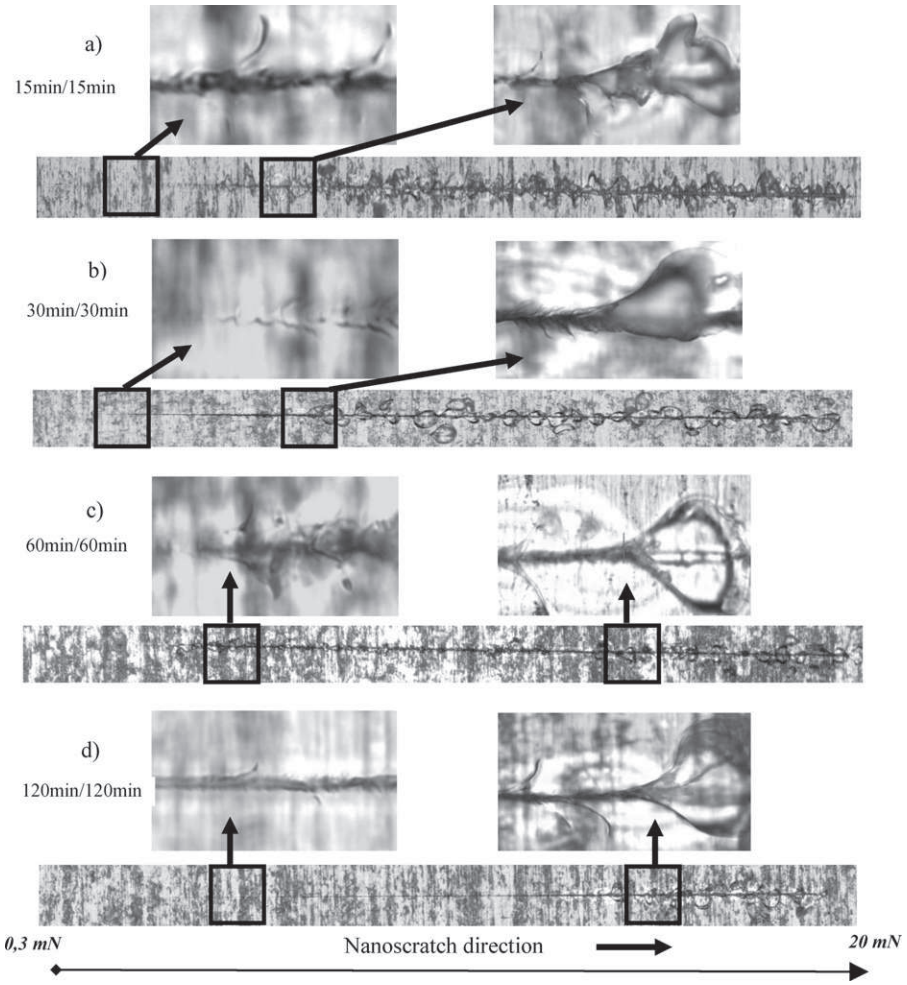

Fig. 13. Optical micrographs of nanoscratches of bi-layered coatings dried at 90 °C, (a) 15 min/15 min, (b) 30 min/30 min, (c) 60 min/60 min and (d) 120 min/120 min.

The best barrier effect is obtained with a double-layered deposit of TEOS–MAP sol with PEG 35000 at 60 g L^{-1} and the pitting potential is equal to the value for AISI 304 stainless steel. Such a system allows to develop covering coatings with the desired anti-corrosive properties. Nevertheless, observations at a macroscopic scale showed that the coatings were insufficiently polymerized because a sticking aspect can be noted. So, this can induce an evolution of the coating under the electron beam during SEM observations. Indeed, the introduction of the PEG 35000 into the sol involves a thickness increase of the coatings but limits the solvents evaporation during drying. That is why, in this case, the "barrier effect" obtained is mainly due to the great hydration and/or solvent saturation of the layers. So, the drying (15 min, 60 °C) for each layer is not sufficient and must be adapted, in particular, time and temperature have been studied and optimized. Eight configurations of drying were investigated (Table 4).

The terminology used to describe the drying conditions is the following: 15 min/15 min, 30 min/30 min, 60 min/60 min and 120 min/120 min at 60 °C or 90 °C.

Initially, measurements of contact angles highlight different evolutions of the wettability of the coatings according to the drying temperature (Fig. 8). At a temperature of 60 °C, wettability towards water of the deposits increases when the drying time increases, which means that the layer becomes less and less solvent saturated. Indeed the sticking phenomenon previously observed indicates that the layers are so much saturated with solvent that water cannot infiltrate any more. The increase in the drying time thus limits this hydration and will generate water infiltration, so the layer becomes more hydrophilic with water. At a temperature of 90 °C, wettability of the coatings towards water decreases when the drying time increases. In this case, the deposits are completely polymerized and denser and denser. So, the porous volume is lower, so water cannot easily incorporate their structure.

That means that by increasing the drying time at 90 °C, dense and water repellent layers can be obtained. So, a drying at 90 °C is more convenient and an optimum of 55° of the contact angle (compared to 49° for a non optimized drying) is reached after a 60 min drying for each layer of the double-layered system.

3.3. Corrosion behavior

Fig. 9 presents the polarization curves in 3.5% NaCl solution of the dried deposits at a temperature of 60 °C compared to bare stainless steel X6Cr17 (AISI 430) and AISI 304. At this temperature, the more the pitting potential ($E_{pitting}$) decreases the higher the drying duration which indicates that hydrated layers present a better barrier effect [19–21]. This is an experimental artefact, because the layers are so much hydrated that even the aggressive NaCl solution cannot infiltrate the coating delaying the appearance of the pits. The problem in this case is the insufficient polymerization state of the coating for future applications.

The study of the polarization curves of the dried coatings at a temperature of 90 °C (Fig. 10) indicates that $E_{pitting}$ potential increases when the drying time increases. Indeed, dryings of 60 min and 120 min allow to obtain a value of $E_{pitting}$ of about 0.250 V approaching the value for stainless steel AISI 304 (0.276 V). That do confirms that dense layers are obtained from 60 min of drying at 90 °C which present better barrier properties that AISI 430 substrate and quite similar properties to those of the AISI 304.

Table 5 indicates the pitting potentials of the coatings for various dryings tested and confirms the tendencies previously explained.

Optimized drying has been determined: 60 min with 90 °C for each of the two layers (60 min/60 min, 90 °C). Such a drying makes possible to obtain homogeneous layers which recover all the surface as shown in Fig. 11.

3.4. Adhesion characteristics

The adhesion of the bi-layered coatings has been evaluated by nanoscratch test by measuring the critical normal load for cracking (beginning of brittle strain) CL1 and the critical normal load for spalling (chipping) CL2 (Chips (flakes) propagating to the substrate and leading to the delamination of the coating are appearing). All test parameters are kept constant for each sample. The critical normal loads are summed up in Table 6.

Microscopic observations of the nanoscratch on the bilayer coatings after a thermal treatment at 60 °C are reported in Fig. 12. If no spalling or delamination can be observed on the coating, the plastic strain can be observed for lower normal load of 0.3 mN and the cracking events are starting for a normal load of 2.9 mN.

This is in good agreement with the previous results showing a poor polymerization of the coating dried at 60 °C.

At this drying temperature the duration of the thermal treatment does not influence the CL1 value but the CL2 value is increasing slightly from 5 to 6 mN (Fig. 13).

Higher critical normal loads CL1 and CL2 are obtained for drying temperature of 90 °C, whatever the drying duration. Even a shorter thermal treatment duration of 15 min is allowing to reach higher critical load values. Therefore the drying temperature of 90 °C has been chosen for the thermal treatment, in order to avoid industrial processing problems at higher temperature.

As for the 60 °C drying, several thermal treatment durations at 90 °C have been evaluated for the bi-layered system. From a drying duration of 60 min/60 min, CL1 and CL2 values are more than doubled compared to 30 min/30 min duration (CL1: 2.2–4.8 mN; CL2: 6.8–14.5 mN). Beyond this 60 min/60 min duration, the CL1 and CL2 values remain almost constant.

4. Conclusion

A new formulation of hybrid coatings containing TEOS and MAP was developed successfully making it possible to cover homogeneously a rough stainless steel AISI 430 substrate by reaching the anti-corrosion properties of AISI 304L stainless steel. The addition of the PEG 35000, used as plasticizer at a concentration of 60 g L^{-1} allows to increase, by a factor of 6, the sol viscosity. In this case, the mass gain and the thickness of the deposits significantly increase improving the barrier effect. Double-layered systems were developed to adjust the thickness but it has been necessary to optimize the drying step in order to obtain polymerized coatings. Thus, a good compromise of drying of 60 min at 90 °C for both layers composing the deposit allows to obtain an efficient system and to increase its hydrophobicity. With such a drying, the barrier effect of the coating is identical to AISI 304L stainless steel used as reference and adhesion with the substrate is highly improved.

References

[1] S. Pathak, A. Khanna, Prog. Org. Coat. 62 (2008) 409–416.
[2] N. Voevodin, V. Balbyshev, M. Donley, Prog. Org. Coat. 52 (2005) 28–33.
[3] A.S. Hamdy, D. Butt, Surf. Coat. Technol. 201 (2006) 401–407.
[4] R.L. Parkhill, E.T. Knobbe, M.S. Donley, Prog. Org. Coat. 41 (2001) 261–265.
[5] Y. Li, A. Ba, M.S. Mahmood, Electrochim. Acta 53 (2008) 7859–7862.
[6] D. Wang, G.P. Bierwagen, Prog. Org. Coat. 64 (2009) 327–338.
[7] C.J. Brinker, G.W. Scherer, Sol–Gel Sci. (1990).
[8] Y. Joshua Du, M. Damron, G. Tang, H. Zheng, C.-J. Chu, J.H. Osborne, Prog. Org. Coat. 41 (2001) 226–232.
[9] C. Brinker, G. Frye, A. Hurd, C. Ashley, Thin Solid Films 201 (1991) 97–108.
[10] X. Zhong, Q. Li, J. Hu, S. Zhang, B. Chen, S. Xu, F. Luo, Electrochim. Acta 55 (2010) 2424–2429.
[11] V. Sarmento, M. Schiavetto, P. Hammer, A. Benedetti, C. Fugivara, P. Suegama, S. Pulcinelli, C. Santilli, Surf. Coat. Technol. 204 (2010) 2689–2701.
[12] A.L.K. Tan, A.M. Soutar, Thin Solid Films 516 (2008) 5706–5709.
[13] A. Galio, S. Lamaka, M. Zheludkevich, L. Dick, I. Müller, M. Ferreira, Surf. Coat. Technol. 204 (2010) 1479–1486.
[14] W.E. Hansal, S. Hansal, M. Pölzler, A. Kornherr, G. Zifferer, G.E. Nauer, Surf. Coat. Technol. 200 (2006) 3056–3063.
[15] F.M. Vanina, P.J.A. Sobrala, F.C. Menegallib, R.A. Carvalhoa, A.M.Q.B. Habitante, Food Hydrocolloids 19 (2005) 899–907 (influence content plastif).
[16] C. Merlatti, F.X. Perrin, E. Aragon, A. Margaillan, Prog. Org. Coat. 61 (2008) 53–62.
[17] M.T. Rodrıguez, J.J. Gracenea, S.J. Garcıa, J.J. Saura, J.J. Suay, Prog. Org. Coat. 50 (2004) 123–131.
[18] Jui-Ming Yeh, Chang-Jian Weng, Wen-Jia Liao, Yi-Wen Mau, Surf. Coat. Technol. 201 (2006) 1788–1795.
[19] C.M. Abreu, M.J. Cristobal, X.R. Novoa, G. Pena, M.C. Peĭrez, Electrochim. Acta 47 (2002) 2215–2222.
[20] G.X. Shen, Y.C. Chen, C.J. Lin, Thin Solid Films 489 (2005) 130–136.
[21] T.E. Graedel, J. Electrochem. Soc. 136 (1989) 193–203.
[22] J. Malzbender, J.M.J. den Toonder, A.R. Balkenende, G. De With, Mater. Sci. Eng., R. 36 (2002) 47–103.
[23] J. Ballarre, E. Jimenez-Pique, M. Anglada, S.A. Pellice, A.L. Cavalieri, Surf. Coat. Technol. 203 (2009) 3325–3331.
[24] A. Pepe, M. Aparicio, A. Duran, S. Ceré, J. Sol–Gel Sci. Technol. 39 (2006) 131–138.